2013

Operational Evapotranspiration Mapping Using Remote Sensing and Weather Datasets: A New Parameterization for the SSEB Approach

Gabriel B. Senay
USGS EROS, senay@usgs.gov

Stefanie Bohms
SGT Inc.

Ramesh K. Singh
ARTS

Prasanna H. Gowda
USDA-ARS

Naga M. Velpuri
ARTS

See next page for additional authors

JOURNAL OF THE AMERICAN WATER RESOURCES ASSOCIATION
AMERICAN WATER RESOURCES ASSOCIATION
Vol. 49, No. 3
June 2013

OPERATIONAL EVAPOTRANSPIRATION MAPPING USING REMOTE SENSING AND WEATHER DATASETS: A NEW PARAMETERIZATION FOR THE SSEB APPROACH[1]

Gabriel B. Senay, Stefanie Bohms, Ramesh K. Singh, Prasanna H. Gowda, Naga M. Velpuri, Henok Alemu, and James P. Verdin[2]

ABSTRACT: The increasing availability of multi-scale remotely sensed data and global weather datasets is allowing the estimation of evapotranspiration (ET) at multiple scales. We present a simple but robust method that uses remotely sensed thermal data and model-assimilated weather fields to produce ET for the contiguous United States (CONUS) at monthly and seasonal time scales. The method is based on the Simplified Surface Energy Balance (SSEB) model, which is now parameterized for operational applications, renamed as SSEBop. The innovative aspect of the SSEBop is that it uses predefined boundary conditions that are unique to each pixel for the "hot" and "cold" reference conditions. The SSEBop model was used for computing ET for 12 years (2000-2011) using the MODIS and Global Data Assimilation System (GDAS) data streams. SSEBop ET results compared reasonably well with monthly eddy covariance ET data explaining 64% of the observed variability across diverse ecosystems in the CONUS during 2005. Twelve annual ET anomalies (2000-2011) depicted the spatial extent and severity of the commonly known drought years in the CONUS. More research is required to improve the representation of the predefined boundary conditions in complex terrain at small spatial scales. SSEBop model was found to be a promising approach to conduct water use studies in the CONUS, with a similar opportunity in other parts of the world. The approach can also be applied with other thermal sensors such as Landsat.

(KEY TERMS: drought; evapotranspiration; irrigation; remote sensing; water use.)

Senay, Gabriel B., Stefanie Bohms, Ramesh K. Singh, Prasanna H. Gowda, Naga M. Velpuri, Henok Alemu, and James P. Verdin, 2013. Operational Evapotranspiration Mapping Using Remote Sensing and Weather Datasets: A New Parameterization for the SSEB Approach. *Journal of the American Water Resources Association* (JAWRA) 49(3): 577-591. DOI: 10.1111/jawr.12057

INTRODUCTION

Evapotranspiration (ET) is an important process in the hydrologic cycle. ET plays a major role in the exchange of mass and energy between the soil-water-vegetation system and the atmosphere. ET comprises two sub-processes: evaporation and transpiration. Evaporation occurs on the surfaces of open water bodies, vegetation, and bare ground. Transpiration

[1]Paper No. JAWRA-12-0097-P of the *Journal of the American Water Resources Association* (JAWRA). Received April 25, 2012; accepted October 25, 2012. **Discussions are open until six months from print publication.**

[2]Respectively, Research Physical Scientist (Senay), USGS Earth Resources Observation and Science (EROS) Center, 47914 252nd Street, Sioux Falls, South Dakota 57198; Geomatic Analyst (Bohms), SGT Inc., Contractor to the USGS EROS Center, Sioux Falls, South Dakota 57198; Scientist (Singh, Velpuri), ARTS, Contractor to the USGS EROS Center, Sioux Falls, South Dakota 57198; Research Agricultural Engineer (Gowda), USDA-Agriculture Research Service, Bushland, Texas 79012; Graduate Student (Alemu), GISc Center of Excellence, South Dakota State University, Brookings, South Dakota 57007; and Physical Scientist (Verdin), USGS EROS Center, Boulder, Colorado 80305 (E-Mail/Senay: senay@usgs.gov).

involves the withdrawal and transport of water from the soil/aquifer system through plant roots and stem, and eventually from the plant leaves into the atmosphere. Knowledge of the rate and amount of ET for a given location is an essential component in the design, development, and monitoring of hydrologic, agricultural, and environmental systems. For example, ET is a key variable in irrigation scheduling, water allocation, crop modeling, understanding water dynamics in wetlands, and quantifying energy-moisture exchange between the land surface and the atmosphere.

According to Senay *et al.* (2011b) a remote sensing-based ET estimation for a basin can be achieved using an integration of methods and data sources. Depending on availability of data and the purpose of ET estimation, different methods can be used. The methods can be grouped into three broad classes: (1) point measurements and some form of regionalization; (2) areal estimates based on weather data and hydrologic modeling; and (3) spatially explicit estimates based on remotely sensed data and modeling. The spatially explicit methods of estimating ET can be further divided into vegetation index (VI)-based and thermal-based approaches. In this study, we present a new simplified parameterization for implementing the thermal-based ET estimation at regional and global scales through a surface energy modeling framework. The new parameterization is designed for operational implementation of the Simplified Surface Energy Balance (SSEB) approach developed by Senay *et al.* (2007). SSEB has been evaluated by comparing it with lysimetric data (Gowda *et al.*, 2009), and by comparing it with the Mapping EvapoTranspiration at high Resolution and with Internalized Calibration (METRIC) model (Senay *et al.*, 2011a) and with water balance-based ET (Senay *et al.*, 2011b).

Surface energy balance methods have been developed and used by several researchers (Jackson *et al.*, 1981; Moran *et al.*, 1996; Anderson *et al.*, 1997; Bastiaanssen *et al.*, 1998; Kustas and Norman, 2000; Roerink *et al.*, 2000; Su, 2002; Allen *et al.*, 2005, 2007a, b; Su *et al.*, 2005; Senay *et al.*, 2007, 2011a, b) to estimate agricultural crop water use and landscape ET. A comprehensive summary of the various surface energy balance models is presented by Gowda *et al.* (2008) and Kalma *et al.* (2008).

The main objective of this study was to introduce a new simplified parameterization to estimate actual ET using predefined boundary conditions for the hot and cold reference pixels so that ET can be estimated operationally as a function of the land surface temperature (Ts) obtained from remotely sensed data and reference ET (ETo) from global weather datasets using the SSEB approach.

JUSTIFICATION

Existing model parameterization in the SSEB and also in the "parent" models such as Surface Energy Balance Algorithm for Land (SEBAL) (Bastiaanssen *et al.*, 1998) and METRIC (Allen *et al.*, 2005, 2007a, b) require setting up the model in uniform hydro-climatic regions where climatic conditions are comparable to the hot and cold reference pixels so as to limit the impact of confounding factors that cause changes in land surface temperature (LST) other than water use differences. Although elevation-induced variations were handled using a lapse rate correction, for continental applications, several model setups would be required to cover the contiguous United States (CONUS). This inhibits automation, as it is time-consuming and introduces artifacts in adjacent regions. The recommended model setup is generally not to exceed an area of 200 km $\times$ 200 km extent.

The SSEB has been implemented successfully for regional applications to monitor and assess the impact of water limited conditions on crop performance. The original formulation of SSEB (Senay *et al.*, 2007) was to apply the thermal data on uniform agro-hydrologic locations such as irrigation basins where the impact of elevation and latitude had little effect on the spatial distribution of ET fractions. However, Senay *et al.* (2011a) enhanced the original SSEB formulation to handle the impact of topography on surface temperature using a lapse rate correction factor. Furthermore, Senay *et al.* (2011b) introduced a revised SSEB that handles both elevation and latitude effect on surface temperature using the difference between land surface temperature (LST; Ts) and air temperature (Ta). In this new parameterization, the user only needs to specify the Ts from remotely sensed data to estimate ET fractions since the boundary for hot and cold reference conditions are predefined for each location and period using a simplified climatological energy balance calculation procedure, as described in the methods section. The new parameterization resembles the Surface Energy Balance System (SEBS) model (Su, 2002), which evaluates the energy balance terms of each pixel at the "wet" and "dry" limiting conditions and actual ET will occur between these two limits. The novelty in the Operational Simplified Surface Energy Balance (SSEBop) model is that the difference between the hot and cold reference values is predefined for a given pixel. The cold reference value is estimated as a fraction of the air temperature and the hot reference value is obtained by adding the predefined temperature difference (dT) to the cold reference value.

The new simplified parameterization is designed to reduce the likelihood of model operator errors that

existed in the previous versions of the SSEB and similar models. With the new modeling approach the most significant error may result due to bias in the use of a constant dT function that is unique for each pixel. However, users are assured that any relative change in the spatial and temporal pattern of seasonal ET is only due to change in the Ts and unlikely from differences in anchor pixels selection and model setup. This is particularly important for the WaterSMART (Water for Sustaining and Managing America's Resources for Tomorrow) project of the U.S. Department of the Interior (DOI)/US Geological Survey (USGS) which plans to estimate year-to-year variability in consumptive use in irrigation basins in a timely manner, i.e., knowledge of the previous year consumptive use estimates needs to be determined before the new irrigation season starts.

This study presents the new parameterization approach, validation results using AmeriFlux data, and annual ET with their anomalies for the CONUS.

MATERIALS AND METHODS

Data

The important datasets required to operationally implement SSEBop are presented in Table 1. The clear-sky net radiation (R_n) was calculated using standard equations recommended by Allen *et al.* (1998). Air temperature data for 2000-2011 was obtained from the Parameter-elevation Regressions on Independent Slopes Model (PRISM) (http://www.prism.oregonstate.edu/; accessed on 12/01/2012). Monthly minimum and maximum Ta a were disaggregated to eight day time scale with a simple moving average process. As part of the supporting dataset for the development of the dT function, the 16 day normalized difference vegetation index (NDVI) from the Moderate Resolution Imaging Spectroradiometer (MODIS) was used. Furthermore, the topographic elevation data were obtained from Shuttle Radar Topographic Mission (SRTM) at 1 km spatial resolution (http://srtm.csi.cgiar.org/; accessed on 12/01/2012). The eight day land surface temperature (Ts) data from 1 km eight day MODIS global LST and emissivity data (Terra MOD11A2.005) product (Wan, 2008) were acquired from the NASA Land Processes Distributed Active Archive Center (LP DAAC) website (https://lpdaac.usgs.gov/lpdaac/get_data; accessed on 18/01/2012) for the available periods from 2000 through 2011. The daily short grass reference ET (ETo) was calculated and made available from the USGS Earth Resources Observation and Science (EROS) Center. The ETo (Senay *et al.*, 2008) was calculated from six hourly weather datasets from the National Oceanic and Atmospheric Administration's (NOAA) Global Data Assimilation System (GDAS) (Kanamitsu, 1989) using the standardized Penman-Monteith equation (Allen *et al.*, 1998). The third dataset includes latent heat flux measurements from eddy covariance (http://public.ornl.gov/ameriflux; accessed on 25/01/2012) flux towers that have been used for validation purposes (Baldocchi *et al.*, 2001). Eddy covariance data (30-minute interval) from 45 AmeriFlux stations (Figure 1) were aggregated to monthly time scale for 2005.

TABLE 1. Summary of Data Types and Purposes for the Parameterization and Operation of the SSEBop Model.

No.	Dataset	Symbol	Source	Purpose
1	Elevation	z	SRTM	Air pressure
2	Temperature correction coefficient	c	PRISM	Tc
3	Land surface temperature	Ts	MODIS	ETf, ETa
4	Air temperature	Ta	PRISM	R_n, Tc, dT
5	Temperature difference	dT	Model	dT
6	Clear-sky net radiation	R_n	Model	dT
7	Reference ET	ETo	GDAS	ETa
8	Aerodynamic resistance	r_{ah}	Model	dT
9	Albedo	α	MODIS	Ts
10	NDVI	-	MODIS	dT

Notes: NDVI, Normalized Difference Vegetation Index; SRTM, Shuttle Radar Topography Mission; PRISM, Parameter-elevation Regressions on Independent Slopes Model; MODIS, Moderate Resolution Imaging Spectroradiometer; GDAS, Global Data Assimilation System.

New Parameterization Approach

A new approach was developed that predefines the temperature difference (dT) between the "hot" and "cold" reference values for each pixel unlike the original SSEB formulation or similar models (e.g., SEBAL or METRIC) that use a set of reference hot and cold pixel pairs applicable for a limited, uniform hydro-climatic region. To estimate ET routinely, the only data needed for this method are Ts, Ta, and ETo. This is a bold proposition, but grounded in the scientific knowledge that most of the surface energy balance process is driven by the available R_n. Since thermal remote sensing is conducted under clear-sky conditions, we argue that the boundary conditions for the hot and cold reference points should not change from year to year or the changes are small in relation to the accuracy level obtained through varying boundary conditions. We hypothesize that the difference between the hot and cold values remains nearly constant for a given location and period (day or eight day) under clear-sky conditions. The cold boundary condition is obtained as a fraction of the Ta. With this basic assumption, we can

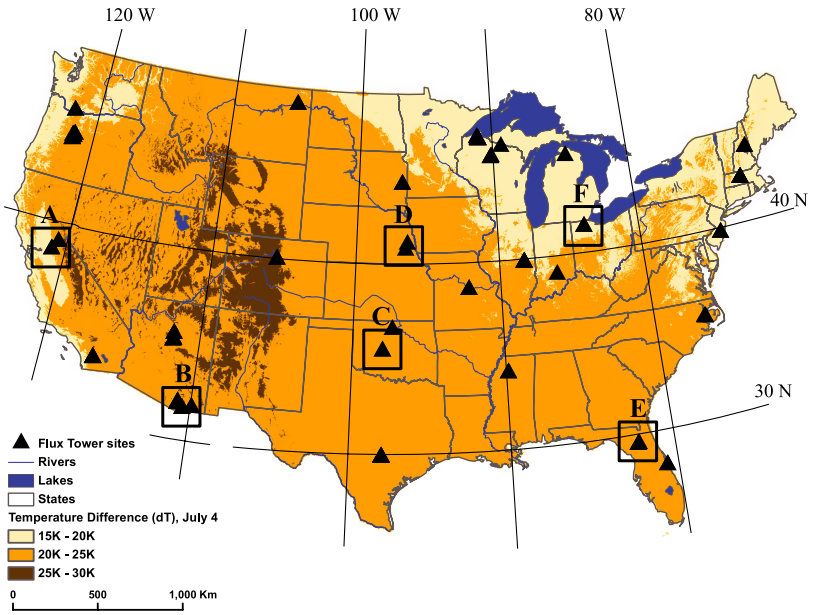

FIGURE 1. Spatial Distribution of dT Values in Three Broad Classes for July 4. Triangular markers indicate location of AmeriFlux stations and lettered-squares show the selected sites used for temporal traces of Ts, Th, Tc, and ET from Operational Simplified Surface Energy Balance (SSEBop) and eddy covariance tower sites shown in Figure 3.

establish the hot and cold boundary conditions for a given pixel and period as a function of largely the net solar radiation under a clear-sky condition.

With this simplification, actual ET (ETa) is estimated using Equation (1) as a fraction of the ETo. The ET fraction (ETf) is calculated using Equation (2).

$$ETa = ETf \times kETo \tag{1}$$

where ETo is the grass reference ET for the location; k is a coefficient that scales the grass reference ET into the level of a maximum ET experienced by an aerodynamically rougher crop. A recommended value for k is 1.2. Alternatively, the actual magnitude of k should be determined using a validation/calibration process using field data such as lysimeter, soil water balance, or energy balance methods since the calculation of the predefined parameters may already incorporate a compensating bias.

$$ETf = \frac{Th - Ts}{Th - Tc} \tag{2}$$

where Ts is the satellite-observed land surface temperature of the pixel whose ETf is being evaluated on a given time period (daily or eight day average for MODIS). Th is the estimated Ts at the idealized reference "hot" condition of the pixel for the same time periods, the cold reference value Tc, is the estimated Ts at the idealized reference "cold" condition of the pixel of the same time period. The difference between Th and Tc is simply the dT that will be discussed later.

Tc Determination

With the new parameterization in SSEBop, Tc for any given period and pixel is approximated as being close (with a correction factor to be discussed later) to the corresponding Ta. This is based on the assumption that for a given clear-sky day or eight day period, the land surface will experience an ET rate equal to the potential rate (healthy, well-watered vegetation, or well-watered bare soil) when its Ts is close to the near-surface air temperature (i.e., little or no sensible heat flux). In the absence of a readily available Ta, the operational processing can be simplified (with a reduction in accuracy) by using a climatological maximum Ta instead of the hourly Ta temperature that corresponds with the satellite overpass time. However, a correction is necessary for using the Ta as surrogate for Tc for two reasons: (1) Ts and Ta are not expected to correspond in magnitude (even at the cold pixel) since the methods and principles of data acquisition are different, but they are expected to correlate well in temporal variability for a given location; (2) the two temperatures will be acquired at different times; the maximum Ta generally occurs in the afternoon (for much of the CONUS in the summer) while the daytime satellite overpass (MODIS, Landsat) for the Ts occurs before noon for this application with a nominal overpass time of 10:30.

The use of Ta for the cold boundary condition is a very important assumption and holds one of two keys for the simplification process. Thus, careful attention

should be given to make sure that the two datasets correspond well. This can be checked using the corresponding *T*s and *T*a from well-watered vegetation in different parts of the study region. When there is a systematic bias in this relationship, a simple correction for bias is performed to solve the problem. In using the MODIS *T*s (daytime Terra MOD11A product), we have determined the *T*c boundary condition using the following correction coefficient.

$$Tc = c \times Ta \tag{3}$$

where *T*a is the near-surface maximum *T*a for the period; *c* is a correction factor that relates *T*a to *T*s on a well-watered, fully transpiring vegetation surface.

The correction coefficient *c* is determined as a seasonal average between *T*s and *T*a on all pixels where NDVI is greater or equal to 0.8 as shown in Equation (4). Exploratory results (Figure 2) showed that this coefficient varied little spatially; therefore, we used a single spatially averaged *c* factor for the entire CONUS for simplicity and with the assumption that the spatial differences were too small for operational application with a major interest in seasonal ET. However, for localized applications, user can develop local-specific "*c*" values.

$$c = \frac{Ts\_cold}{Ta} \tag{4}$$

where *T*s_cold is the satellite-based *T*s at the cold pixel where NDVI > 0.8 and *T*a is the corresponding daily maximum air temperature at the same location and period. The correction was calculated as the spatially averaged values of the available locations. These areas are usually obtained during the growing season (March to September) from irrigated areas and forested regions. The value of this correction factor was determined to be 0.993 when both MODIS *T*s and *T*a were processed in Kelvin units (Figure 2). The one standard deviation (0.00796) envelope in Figure 2 represents the average variations from up to 20 data points in each eight day period that met the condition of NDVI > 0.8, resulting in coefficient of variation (CV) less than 1.0%. The temporal pattern in Figure 2 shows that the "*c*" coefficient is steady throughout the season indicating the reliability of using a single coefficient in space and time.

Predefined d*T and Hot Boundary Condition*

Once the *T*c is defined as the fraction of the *T*a, the hot boundary condition (*T*h) can also be defined by a constant difference (d*T*) that will be added to the *T*c of each pixel on a given time period. The observed d*T* (difference between hot and cold boundary condition) during the peak crop growing season has been observed to be in the order of 20 K (roughly varying between 15° and 25° based on location, in most cases (evaluated using *T*s data in United States (U.S.), Africa, and Afghanistan by Senay *et al.*, 2007, 2011a). Similar d*T* ranges have been reported by Qiu *et al.* (1998). In this new parameterization, the innovative approach is to use a predetermined seasonally dynamic d*T* that is unique to each location anywhere in the world. Thus, the second key component of the simplification is in the estimation of d*T* from energy balance principles for a clear-sky condition. Clear sky is specified because that is an important condition for the usefulness of the thermal-based remote sensing ET estimation.

The predefined d*T* is solved from the R_n equation for a bare, dry soil where ET is assumed to be 0 and sensible heat is assumed to be maximum (Bastiaanssen *et al.*, 1998; Allen *et al.*, 2007b). The radiation balance for a bare, dry soil can be written as follows:

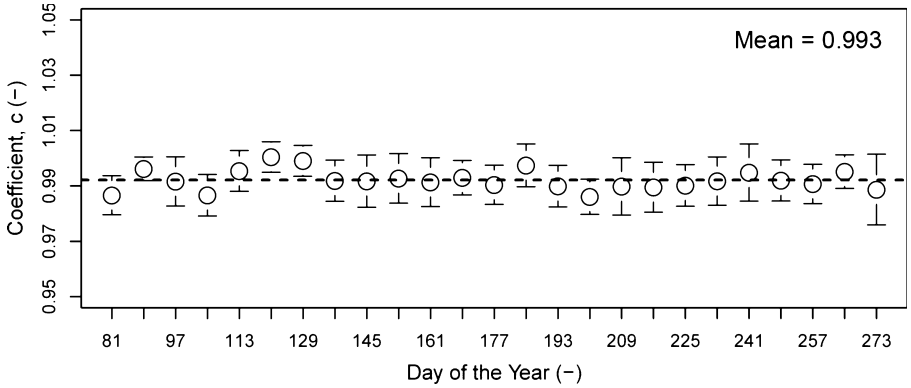

FIGURE 2. Calibration Coefficient (c) for Relating Cold Pixel Temperature (*T*c) with PRISM-Based Maximum Air Temperature (*T*a) (n = 2,174).

$$R_n = LE + H + G \quad (5)$$

where LE is the latent heat flux (equivalent to ET with the use of the heat of vaporization, L, and the density of water), H is the sensible heat flux (W/m^2), and G is the ground heat flux (W/m^2). Since LE and G are considered 0, the magnitude of the R_n can be equated with the sensible heat equation as:

$$R_n = H = \frac{\rho_a \times C_p \times dT}{r_{ah}} \quad (6)$$

where ρ_a is air density (kg/m^3), C_p is specific heat of air at constant pressure (~1.013 kJ/kg/K), and r_{ah} is the aerodynamic resistance for heat (s/m). Since all R_n is now assumed to be used for sensible heat flux at the hot boundary condition, H will be approximated by the clear-sky net radiation received at an idealized bare and dry surface for a given pixel during a given period. The next step is to estimate the available clear-sky net radiation that is available for a given period so that dT can be solved by rearranging Equation (6) as shown in Equation (16).

Clear-sky net radiation is estimated using a series of equations as presented with the Food and Agricultural Organization (FAO) publication number 56 (Allen *et al.*, 1998). R_n is estimated as the difference between net shortwave (R_{ns}) and the outgoing net long-wave radiation (R_{nl}).

$$R_n = R_{ns} - R_{nl} \quad (7)$$

$$R_{ns} = (1 - \alpha)R_s \quad (8)$$

where R_{ns} (MJ/m^2/d) is net solar or shortwave radiation; α is the albedo. A value of 0.23 for α is recommended. R_s (MJ/m^2/d) is incoming solar radiation.

$$R_s = (0.75 + 2 \times 10^{-5} \times z)R_a \quad (9)$$

where R_a is extraterrestrial radiation (MJ/m^2/d); 0.75 is a suggested correction coefficient in the absence of measured data to represent a fraction of R_a reaching the surface of the earth on clear days, and z is elevation (m) (Allen *et al.*, 1998).

R_a for each day of the year and a given modeling pixel (latitude) can be estimated from a solar constant, the solar declination and time of the year (Allen *et al.*, 1998).

$$R_a = \frac{24 \times 60}{\pi} G_{sc} d_r [\omega_s \sin(\varphi)\sin(\delta) + \cos(\varphi)\cos(\delta)\sin(\omega_s)] \quad (10)$$

where, G_{sc} (0.0820 MJ/m^2/min) is solar constant, d_r (-) is inverse relative earth-sun distance, Equation (11), and δ (rad) is solar declination, Equation (12). The latitude ϕ (rad) is positive for northern hemisphere and negative for southern hemisphere. ω_s (rad) is sunset hour angle, Equation (13). The inverse relative earth-sun distance, d_r is given by the equation:

$$d_r = 1 + 0.033 \times \cos(\frac{2\pi}{365}J) \quad (11)$$

The solar declination angle δ is given by the following:

$$\delta = 0.409 \sin(\frac{2\pi}{365}J - 1.39) \quad (12)$$

where J is the day of the year, between January 1st and December 31st.

The sunset hour angle ω_s is given by the equation:

$$\omega_s = \arccos[-\tan(\varphi)\tan(\delta)] \quad (13)$$

To solve Equation (7), we also need the estimation of R_{nl}. There are several equations to estimate R_{nl}; due to its simplicity and availability of limited data, we use the one proposed by FAO 56 in Allen *et al.* (1998). Because the boundary conditions are established under the assumption of clear sky, R_{nl} is estimated as

$$R_{nl} = \sigma\left(\frac{T_{max}^4 + T_{min}^4}{2}\right)(0.34 - 0.14\sqrt{ea})(1.35(\frac{R_s}{R_{so}}) - 0.35) \quad (14)$$

where R_{nl} is net long-wave radiation (MJ/m^2/d); σ is Stefan-Boltzmann constant (4.903×10^{-9} MJ/K^4/m^2/d); T_{max} and T_{min} are maximum and minimum absolute temperature (K), that is K = °C + 273.16; R_s/R_{so} is the relative shortwave radiation (≤ 1.0) where R_s is the calculated solar radiation, Equation (9), based on the cloudiness factor; R_{so} is the calculated clear-sky radiation. In this case, the ratio R_s/R_{so} becomes 1.0 due to the assumption of clear-sky boundary condition; ea is the actual vapor pressure (kPa) estimated using the following Equation (15).

$$ea = e^o(T_{min}) = e^{\left(\frac{17.27 \times T_{min}}{T_{min} + 237.3}\right)} \quad (15)$$

where e (T_{min}) is the saturated vapor pressure that is occurring at daily minimum temperature (T_{min};°C). Allen *et al.* (1998) recommends the use of dew point temperature (approximated by T_{min}) for the estimation of e^o when humidity data are not available or of questionable quality for well-watered conditions.

Although the assumption of equating the minimum temperature to the dew point is only valid in well-

watered conditions, we assume that this will serve the purpose of establishing generalized boundary conditions, considering the many simplifications in the approach. Furthermore, both $T_{\min}$ and $T_{\max}$ in Equation (15) are based on climatological data. Most of these data are available in monthly time steps; therefore, using smoothing and disaggregation, eight day values were generated to calculate R_{nl} at finer time scales. Once R_{n} is estimated for each pixel at 1 km scale, we solved for the predefined dT using the following Equation (16), a rearranged form of Equation (6).

We solved for dT for each eight day period using R_{n}, C_p, and ρ and r_{ah} as follows:

$$\mathrm{d}T = \frac{R_{\mathrm{n}} \times r_{\mathrm{ah}}}{\rho_a \times C_p} \tag{16}$$

where C_p is the specific heat of air at constant pressure (1.013 kJ kg^{-1} °C^{-1}); ρ_a is the density of air which is calculated using Equation (17) (Allen *et al.*, 1998); r_{ah} is the aerodynamic resistance to heat flow from a hypothetical bare and dry surface; r_{ah} was determined through a quasi-calibration process as explained later.

$$\rho_a = \frac{1000P}{T_{kv}R} = 3.486\frac{P}{T_{kv}} \tag{17}$$

where ρ_a is the air density (kg m^{-3}); R is the specific gas constant (287 J kg^{-1} K^{-1}); T_{kv} is the virtual temperature, a temperature at which dry air must be heated to equal the density of moist air at the same pressure. For the average condition (*ea* in the range of 1-5 kPa and P between 80 and 100 kPa), Allen *et al.* (1998) recommend the use of $T_{kv} = 1.01\ (T + 273)$ where T is the mean daily temperature (°C).

$$P = 101.3\left(\frac{293 - 0.0065 \times Z}{293}\right)^{5.26} \tag{18}$$

Assuming atmospheric pressure at sea level is 101.3 kPa, 293 is reference temperature (K) at sea level, Z is elevation (m) obtained from 1 km global digital elevation model (DEM) derived from the SRTM dataset.

Obviously, given a set of field dT values (obtained from Ts imagery as the difference between the hot and cold pixel values), the r_{ah} magnitude will depend on the R_{n} calculation since the other parameters are relatively stable or change in small magnitude. A trial-and-error approach was used to determine the r_{ah} value for SSEBop. This was done by inspecting the r_{ah} value that matches the dT differences observed between the observed hot (bare areas) and cold (vegetated) Ts values in several well irrigated basins in the western U.S. during the peak growing season (California Central Valley, Idaho Snake River Valley, Texas Pan Handle, and Nebraska).

During the peak summer season, field dT values varied between 20 and 25 K depending on the location. Similar differences between dry soil and air were reported by Qiu *et al.* (1998). In our study, by rearranging Equation (6), the average value of r_{ah} from these locations over several months was found to range between 100 and 120 s/m. A comparison with eddy covariance method ET in 2005 showed that an r_{ah} value of 110 s/m produced a reasonable agreement and we decided to fix the r_{ah} value at 110 s/m. Qiu *et al.* (1998) showed that r_{ah} of a dry soil is spatially uniform. Earlier, Calder (1977) stated that the improvements obtained by varying r_{ah} with wind speed may be small. Qiu *et al.* (1998) showed the r_{ah} values for a drying soil surface (bare area with different levels of soil moisture) to be in the range between 60 and 120 s/m, indicating the dry part of the r_{ah} value being close to the higher end.

This suggests that our r_{ah} value of 110 s/m for the dry boundary condition can be used for a useful operational estimation of ET in this method where the interest is the use of remotely sensed thermal data for a quick and consistent estimation of ET and relative ET changes (compared to other years and locations) using one single variable alone, that is as a result of changes in land surface temperature. Furthermore, comparison with 45 eddy covariance tower ET in 2005 showed that 110 s/m gives a reasonable agreement and we chose to fix the r_{ah} value at 110 s/m.

Note that a different R_{n} calculation method will likely require a different estimation procedure for r_{ah}. However, the most important point is that once a r_{ah} is fixed, the dT equation can be applied to any location and season to obtain a location-specific and seasonally varying dT that is expected to occur under clear-sky conditions. The minimum dT occurs in the winter and it rarely falls below 2 K. Since the accuracy of the method reduces at lower dT and does not make physical sense to have a negative dT for a relevant ET estimation, we have limited the minimum dT to 1 K.

Therefore, once the expected dT is determined, the hot boundary condition can be defined simply by adding the dT to the Tc as shown in Equation (19).

$$Th = Tc + dT \tag{19}$$

*T*s *Conditioning for High Albedo Surfaces*

The described method works well in most vegetated and partially vegetated surfaces where albedo values are generally in the range between 0.15 and

0.30. Under these conditions, the change in Ts is less sensitive to the changes in albedo (Roerink *et al.*, 2000). However, in certain land cover types where albedo values are greater than 0.28, the radiometric temperature tends to decrease linearly, potentially due to reduced net radiation. These are generally observed in desert white sands of New Mexico and parts of the Sahara Desert. Although there is not much vegetation cover in these areas, a Ts-based analysis will result in an erroneous interpretation of the image since these locations appear relatively cooler in the Ts image; thereby producing spurious ETf and ETa estimations. To address this problem, one needs to develop a mask or a correction factor to avoid producing spurious colder Ts values that will lead to greater ET fractions and exaggerate the ET from the landscape. In this study, we have developed a simple linear equation that would modify the Ts of these surfaces before the Ts image is used in Equation (20).

For the case of MODIS images, most snow-free vegetated surfaces will have an albedo value less than 0.25, so a correction is applied for areas with albedo > 0.25.

$$Ts_{\text{corrected}} = Ts + 100(\alpha - 0.25) \qquad (20)$$

where α is the broadband albedo as reported in the MODIS dataset; Ts is the reported Ts image value (K); and $Ts_{\text{corrected}}$ is the corrected Ts value (K) which will increase the Ts value in a greater albedo area.

Again, the value of this correction is to modify results from non-vegetated surfaces that may exhibit lower Ts than the expected value. The lower than expected Ts values can be caused by either poor parameterization of the emissivity values in MODIS or lack of the SSEBop model in solving for the full energy balance equation at the surface. More research is required to identify and correct such areas.

*T*s *Conditioning for High Emissivity Bare Areas*

Similarly, areas with high emissivity such as dark lava rocks tend to have low thermal Ts values from imagery. Although this temperature index method works well when the emissivity is around 0.97, high emissivity surface types tend to have smaller Ts than the surrounding region. The lower Ts is not generally accompanied by changes in the Ta, thus tend to create a lower ETf. These areas are generally located in dark rock features such as lava rocks in parts of east Africa, parts of Nevada, and the mountains in the Sahara Desert. These areas need to be treated differently or they will produce a spuriously high ETf and thus a high ET. For these areas solving the energy budget with surface temperature is required as opposed to estimating the net long-wave radiation and the net radiation from proxy air temperature parameters.

For both high albedo and high emissivity areas either a mask needs to be created or a correction factor be applied to avoid spurious ET results. These areas are relatively easy to spot and generally contribute little to seasonal ET totals due to lack of rainfall and vegetation in the first place. The case of water bodies is slightly different. These tend to have lower Ts than the reference cold pixel that is based on the climatological air temperature. Because of this, the ETf remains close to 1 or slightly higher; thus, the ET of a water body is simply a function of the reference ET which also needs correction for magnitude since the energy balance of a water body and a reference crop differ greatly because of major differences in R_n and G.

Summary of the SSEBop Setup Procedures

1. Obtain land surface temperature (Ts) or brightness temperature from remotely sensed imagery (spatial data). This could be instantaneous (Landsat, MODIS) or period-averages such as the eight day Ts from MODIS.
2. Obtain air temperature (Ta) grids as available. Corresponding daily, weekly, or monthly maximums can be used (spatial data). Station data can be used for a small study area such as an irrigation district, representing a uniform climatic region.
3. Establish a correction factor that relates Ts cold with Ta under clear-sky conditions for well-watered, fully vegetated pixels (NDVI > 0.8) (coefficient).
4. Develop dT under clear-sky conditions for each location and time period (seasonally dynamic but annually static) using energy balance equations and r_{ah} for a dry, bare surface, Equation (16) (spatial data).
5. Obtain reference ET for the desired period of actual ET estimation (spatial data). Similar to #2, station data can be used.
6. Compute ETf according to Equation (2) (spatial).
7. Use Equation (1) to estimate actual ET for the given period and create monthly and seasonal aggregation as desired (spatial).

Analysis Procedures

Once the dT values for each 1 km pixel and eight day period were estimated, the SSEBop model was

run for 12 years from 2000 till 2011 to produce eight day ETf, and the corresponding ET. Missing *T*s values were handled as described here. When, in a given eight day period, ETf could not be calculated for a given pixel due to cloud problems (too low *T*s), then the previous-period eight day fraction or next eight day (during reanalysis) are used. In rare cases, if both the previous and next-period are cloudy pixels then a historically calculated median ETf value for that period is used to fill the data gap. From eight day ET totals, monthly and annual ET summaries were created for the CONUS. Median monthly and annual summaries were also created from the 12 year dataset so that monthly and annual anomalies could be created as a percent of the median values of the corresponding aggregation period (monthly and annual sums). The eddy covariance data from 45 stations representing different land cover types were used to evaluate the performance of the SSEBop monthly ET output for 2005 using correlation statistics and scatter plots. Traces of the seasonal *T*h, *T*c, and *T*s distribution were plotted for selected eddy covariance tower sites. Similarly, the monthly traces of eddy covariance tower ET and SSEBop estimated ET is shown for same locations. Scatter plots, correlation statistics, and root mean square error (RMSE) are shown for quantitative evaluations. In addition, annual ET, and ET anomaly graphics were created for visual interpretation of the year-to-year ET changes across the CONUS during the available MODIS years (2000-2011).

RESULTS

Model results are mainly summarized as seasonal ET totals and their anomalies for 2000-2011. Monthly traces of ET are shown for selected sites for demonstration purposes. In addition, eight day traces of the hot and cold boundary conditions and the associated d*T* (difference between hot and cold) are also shown for the selected eddy covariance tower stations.

Figure 1 shows a broad distribution of the d*T* function in the CONUS for one time period (July 4). It can be observed that most of the vegetated regions show d*T* values in narrow ranges between 20 and 25 K. The higher d*T* values (25-30 K) are generally in the western, mountainous regions. The lower ranges of d*T* values (15-20 K) are found in the northeast, probably due to a combination of lower incoming shortwave radiation for the northeast or higher longwave radiation in the high temperature valleys that tends to reduce the net radiation. For the same *T*s and *T*c, areas with higher d*T* will have a higher ET fraction than areas with lower d*T* according to Equation (2). The relative spatial pattern tends to remain the same in the other months (data not shown), but the magnitude of d*T* decreases in the winter months due to reduced net radiation. Also, Figure 1 shows the location of the eddy covariance flux tower sites used for validation and lettered-squares indicate the selected sites for monthly traces of *T*h, *T*s, *T*c, and ET.

Figure 3 shows the temporal variation in *T*h, *T*c, and *T*s on the left panel and the corresponding SSEBop ET and the eddy covariance ET estimates on the right panel. In addition, Figure 4 shows the scatter plot of the pooled monthly datasets from 45 eddy covariance sites that were used to validate the SSEBop model results for the same time period. As expected, the *T*s curve generally lies between the boundary conditions (*T*h and *T*c curves) except for the winter months (Figure 3). In a given period when the *T*s is close to the hot boundary condition (*T*h), the corresponding ET fraction and ETa estimates will be lower, becoming 0 at *T*s = *T*h. On the other hand, when *T*s is close to the cold reference condition (*T*c), ETf will be higher and becomes 1.0 at *T*s = *T*c. On rare situations when *T*s is beyond the boundary conditions, ETf is set to the closest boundary condition at 0 or 1. In this study, this situation occurred mostly in the winter months (e.g., Figure 3D left panel). The main reason for this is probably cloud contamination or snow cover that makes the *T*s colder than the expected reference temperature. These tend to occur either in winter months when ETa is low or in rainfall-rich areas with frequent cloud occurrences in which case the use of ETf = 1 will be acceptable since these are energy-limited environments. Therefore, at ETf = 1, ETa will equal the reference ET under water unlimited condition. In some desert areas when the *T*s becomes more than *T*h, a negative ETf value will be set to 0 and thus assigning 0 for ETa.

Generally, SSEBop was able to capture the seasonality well with strong correlation for individual stations (R^2 between 0.70 and 0.97). However, in terms of magnitude, the specific agreement (overestimation or underestimation) seems to vary from station to station and from season to season. For example, in Tonzi Ranch, California (Figure 3A, right panel) the R^2 is 0.72 but the SSEBop overestimates during the summer months; in Audubon, Arizona (Figure 3B, right panel) the R^2 is 0.83 and generally in good agreement throughout the season; in SGP, Oklahoma (Figure 3C, right panel) the R^2 is 0.95, with an overestimation during the peak summer months; in Mead, Nebraska (Figure 3D, right panel) the R^2 is 0.97 with an underestimation in the early and late summer months; in Austin Cary, Florida (Figure 3E, right panel) the R^2 is 0.89 but there is a large overes-

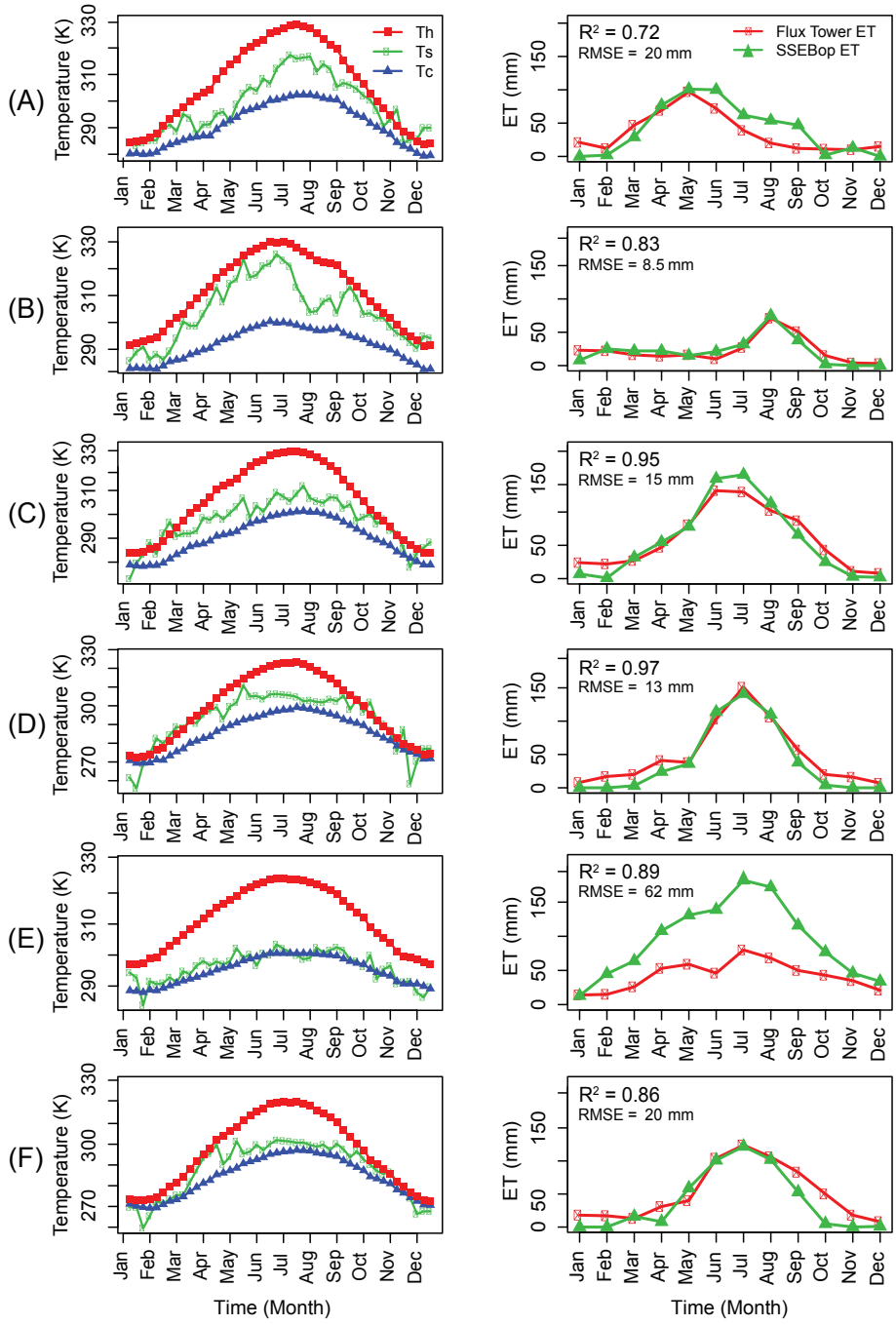

FIGURE 3. Temporal Traces of Eight Day Average *T*s, *T*h, *T*c (left panel) and Monthly SSEBop ET and Eddy Covariance Flux Tower ET (right panel) for Six Locations: (a) Tonzi Ranch, California; (b) Audubon, Arizona; (c) ARM_SGP_Burn, Oklahoma; (d) Mead Rainfed, Nebraska; (e) Austin Cary, Florida; and (f) Oak Openings, Ohio.

timation throughout the year; and in Oak Openings, Ohio (Figure 3F, right panel) the R^2 is 0.86 with an underestimation toward the end of the season in the fall. A close examination is required for the Austin Cary, Florida station, in case the flux tower is rather underestimating since this is generally a wet location with the *T*s being close to the cold reference temperature (*T*c) as shown in Figure 3E, left panel.

Figure 4 shows the scatter plot when the pooled dataset from all 45 eddy covariance sites is correlated with SSEBop monthly ET output for 2005. As shown in Figure 4a, there is quite a large scatter around the one-to-one line. However, there is a reasonable relationship with an R^2 of 0.64 and a 0.99 slope. Although there is a wide scatter about the one-to-one line, getting an R^2 of 0.64 and a slope

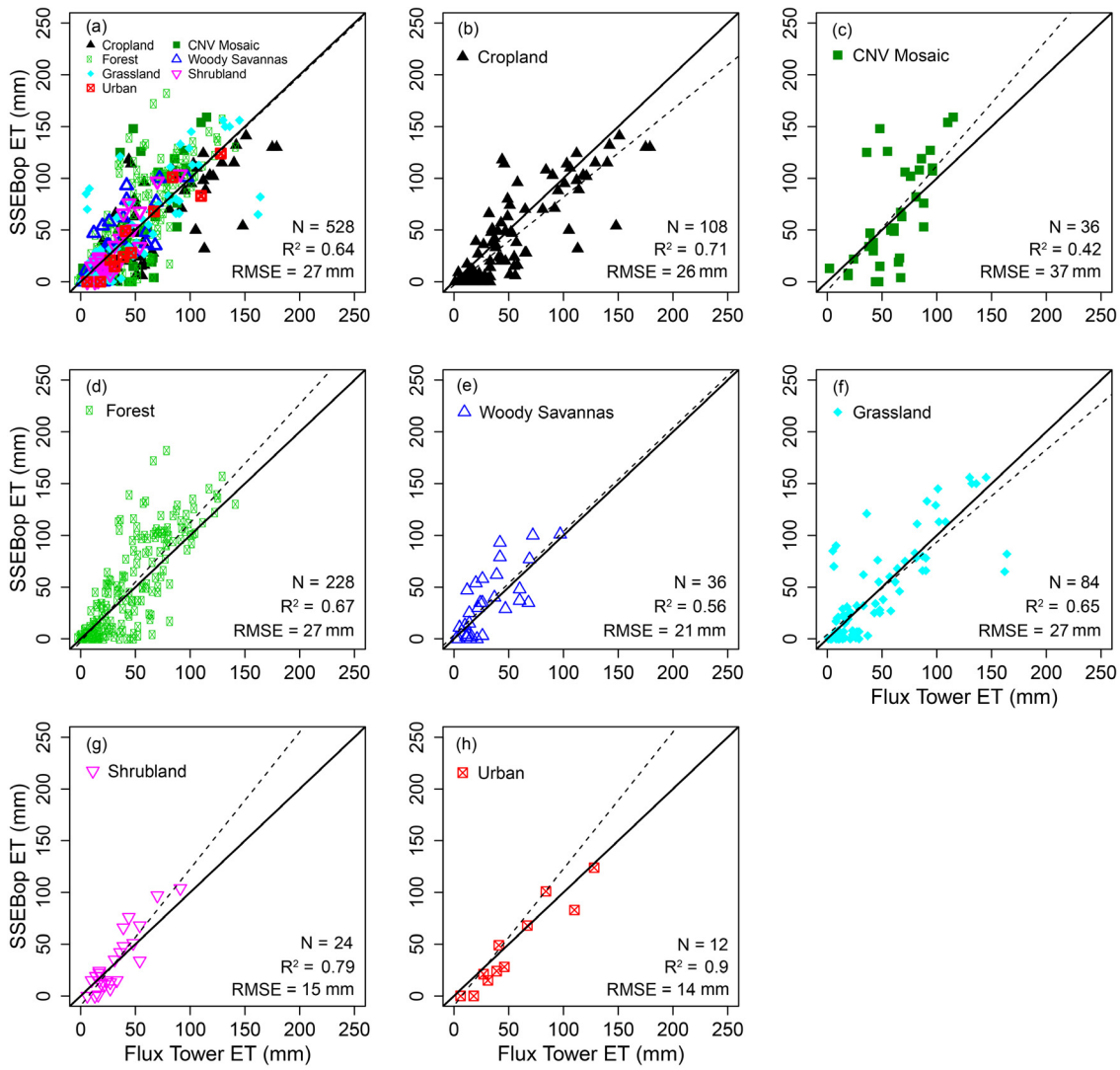

FIGURE 4. Scatter Plot of Monthly Eddy Covariance Flux Tower Data and SSEBop from 45 AmeriFlux Stations Across the CONUS, Covering Diverse Ecosystems Including Cropland, Cropland/Natural Vegetation Mosaic (CNV), Forest, Woody Savannas, Grassland, Shrubland, and Urban.

close to 1.0 for geographically diverse stations having different land use/land cover was encouraging. Separate plotting of modeled and measured monthly ET for different land cover classes (Figures 4b-4h) has shown that SSEBop model performed well for almost all the classes. The results are promising when we consider the limited parameterization in the model and the diversity of the ecosystems the eddy covariance tower stations represent. We have to note that some of the scatter can also be a result of the errors associated with the eddy covariance tower stations and the reference ET calculated from coarse GDAS fields. Although not used in this study, the use of daily in place of monthly maximum *T*a will further improve the model performance. Further investigation is required to understand the response of the SSEBop model for each ecosystem over multiple years and quantify the uncertainty associated with the performance of the model in the different ecosystems.

At this point, with a reasonable match between SSEBop and AmeriFlux stations (explaining 64% of the variability across the CONUS), the SSEBop model can be used to detect seasonal or annual ET anomalies with a high degree of reliability. Particularly, the ET anomaly is reliable since the subjective selection of hot and cold reference pixels is eliminated and the only variable from year to year is the land surface temperature. We also compared the difference between running the SSEBop with yearly varying ETo against using climatological ETo where the average of the available ETo years (2000-2011) were used to create the short-term climatology for each eight day period. The results (comparison not shown) indi-

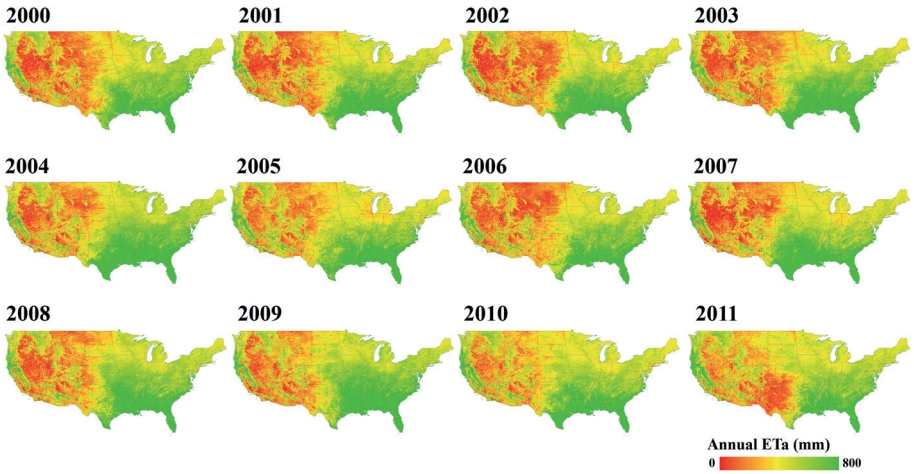

FIGURE 5. SSEBop Estimated Annual ET Distribution Across the CONUS for 12 Years from 2000 to 2011. In general ET maps show high ET values in the southeast, northwest, and forested regions. The maximum value is capped at 800 mm to highlight the ET from agricultural areas that do not exceed 700 mm in most areas. However, the ET from the southeast exceeds 1,000 mm due to high energy and water availability.

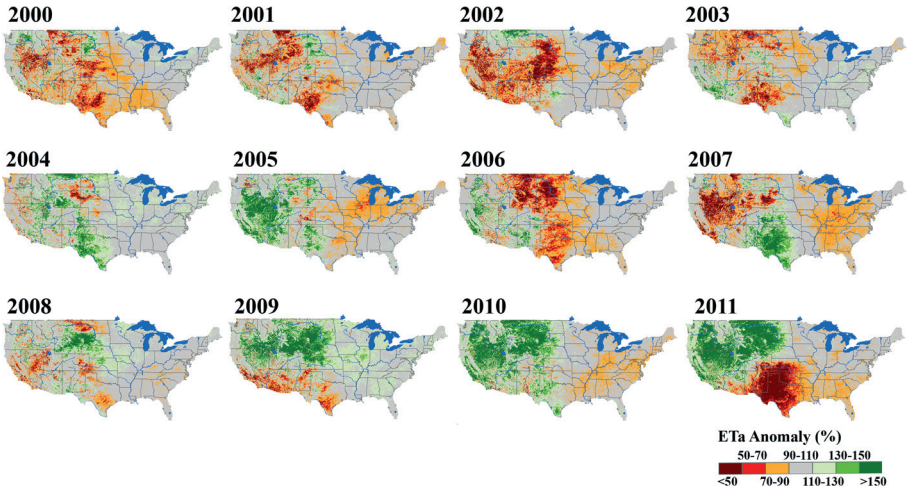

FIGURE 6. SSEBop Annual ET Anomaly for the Period Between 2000 and 2011. Anomalies were created as a percent of each year's total ET in comparison with an annual median ET of 10 year period (2001-2010). The known drought years show clearly, highlighting the potential of the SSEBop for drought monitoring without the need for further parameterization.

cated that using climatological ETo provided a more accurate depiction of the severity of major drought years in known regions such as the 2007 drought in the southeastern U.S. This could be due to the fact that the boundary conditions are established under clear-sky conditions where higher ETo tends to occur. In the case of drought years, where cloud-cover is less, the use of current year ETo was producing much higher actual ET, thus reducing the severity of the expected negative (lower) ET anomaly. Thus, at least for drought detection, we feel using the climatology ETo was producing a more reasonable magnitude. Further research is needed to explain the difference between using yearly varying versus a climatological ETo and its impact in drought detection or to quantify water budget terms.

Figures 5 and 6 show annual ET (Figure 5) and the corresponding ET anomalies (Figure 6) for the CONUS for the period 2000-2011. The close-up spatial patterns of annual ET correspond well with major vegetated regions of the southeast, northwest, and in capturing the higher ET areas in the irrigated basins of Central Valley, California; Snake River Valley, Idaho; and the High Plains aquifer, Texas (Figure 7). As expected, the anomalies in most irrigated areas are closer to the average than nonirrigated areas, which are more affected by the annual rainfall variability. Although the actual magnitude of the

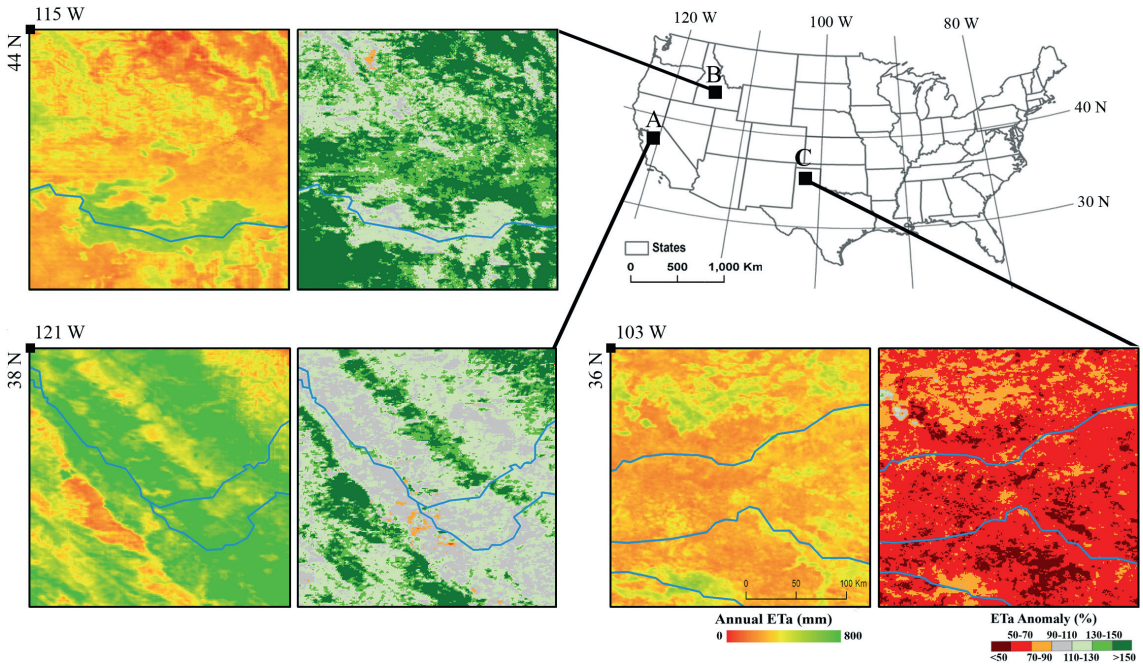

FIGURE 7. A Close-Up of the Annual ET and ET Anomaly Maps for 2005 Show High ET Areas (left panel) and Corresponding ET Anomaly (right panel) in the Irrigated Regions of Central Valley, California (A); Snake River Valley, Idaho (B); and High Plains in Texas (C).

annual ET can be improved with more localized parameterization for establishing the one-time boundary conditions (dT), the existing operational setup is promising for use in change detection and drought monitoring whether the year-to-year water use changes are caused by rainfall deficiency, reduction in the use of irrigation applications, and/or other causes such as fire, diseases, and pest infestations. The major drought years of the United States and their locations and relative severity are depicted well in Figure 6. The results correspond with those reported by the drought monitor (http://droughtmonitor.unl.edu/; accessed on 15/02/2012). For example, the drought years of 2002 (western US), 2006 (High Plains), 2007 (Southeast), and 2011 (Texas and Oklahoma) are well represented.

Again, this shows that the SSEBop is a viable approach that can produce reliable results with minimal effort, in near real-time as soon as the Ts data are available with an automatic processing and posting.

DISCUSSION

It is important to note the requirements in the method as discussed above. While the method eliminates the subjective errors that are introduced during the hot and cold reference selection, the accuracy of the method depends on the accurate representation of the corrected maximum air temperature as a surrogate for the idealized cold LST. This also implies that a high spatial resolution Ta dataset will capture the spatial variability of the study region. A uniform correction factor of 0.993 was used when both the Ts and Ta max are used in Kelvin temperature scale. This correction coefficient can slightly vary depending upon the datasets used. Hence, users who want to apply the method for small irrigation basins are advised to cross-check and establish their own locally specific correction factor if required. The most important point is to realize the possibility of using a fraction of the air temperature as the cold reference point.

Furthermore, the dT is currently calculated using climatological air temperature for both long-wave radiation and for vapor pressure calculation. An improved parameterization for both may provide a more reliable dT, but that will require a sensitivity analysis. The major limitation of the method will show on surfaces with albedo and emissivity values that are different from vegetated surfaces. These surfaces seem to affect both the calculation of the land surface temperature and the resulting ET calculation in the SSEBop approach. Since the SSEBop does not fully solve the individual energy balance components for each pixel, surfaces that have a different energy balance characteristic than a typical soil-vegetation surface found in agricultural areas may not be represented well in the generic SSEBop approach. These places would require location-specific

parameterization so that the energy balance equation is solved more correctly for the dT function. Such places include desert sands with high albedo and dark-colored mountains with high emissivity. In SSEBop, the ET of water bodies is generally driven by the reference ET since the LST of most water bodies is cooler than the air temperature that is used as a surrogate for the cold reference point.

For mountainous regions, further improvement can be achieved in the dT calculation by taking into account slope and aspect in the net radiation calculation. In addition, the current parameterization assumes a constant lapse rate of 0.0065°C/m for air density calculations Equations (17) and (18) and the validity of this assumption requires further sensitivity analysis. In the current product (Figure 1), we have observed a generally high dT (>25 K) in the mountain areas that tend to provide a higher ET fraction for the same Ts *and* Tc. The resulting ET from high elevation areas is higher than expected, highlighting a need to re-parameterize the dT calculation by taking into account the impact of elevation, slope, and aspect. However, even for these kinds of surfaces (deserts and mountains), the SSEBop ET anomaly can be used to detect relative changes, although the absolute magnitude will have a significant estimation bias that needs to be quantified and adjusted before using it for hydrological applications. In addition, the use of crop reference for alfalfa reference ET will bring a significant difference (up to 20%) in the magnitude of ET. However, since this tends to be a constant multiplier, it is important that the SSEBop ET is validated and calibrated with available data such as bias-corrected eddy covariance flux towers or water balance approaches for a given dT function before using the modeled ET in absolute sense for water budget analysis.

CONCLUSIONS

The main objective of this study was to introduce a new simplified parameterization to estimate actual ET using predefined boundary conditions for the hot and cold reference pixels for operational applications.

The use of constant dT has been shown to work reasonably well. The comparison of the modeled ET and eddy covariance flux tower ET from 45 stations, covering diverse ecosystems across the CONUS, resulted in an R^2 of 0.64. Considering the minimal requirements to set up the model and the reliability of obtaining the same result irrespective of the model user, this level of agreement is encouraging at the national scale. This means that, with a more local-specific parameterization of the dT function, improved performance of the SSEBop model can be achieved as shown in selected AmeriFlux tower sites. Furthermore, the use of daily instead of a monthly climatological Ta with a higher spatial resolution (better than the current PRISM 4 km) is expected to improve the performance of SSEBop. Therefore, modelers, interested in estimating consumptive use operationally in irrigated basins, will only need to specify the Ts from remotely sensed imagery to estimate ET of a given field once the dT function is determined and Tc value is estimated as a function of Ta.

Particularly, the SSEBop is a powerful method for detecting changes and anomalies quickly and reliably. The ET anomalies depicted the major drought years and their relative severity in known years from 2000 through 2011. The study also stresses the need to validate and, if necessary, calibrate the absolute magnitudes using eddy covariance flux tower data or water balance approaches before using the results in water budget studies.

More research is required to evaluate the performance of the SSEBop model using more years of data and by using it in other parts of the world. Particularly, it is important to conduct an uncertainty analysis of the approach in estimating dT and its impact on the ET calculations. Furthermore, more work is needed in conducting ET estimation from topographically complex areas and high albedo and emissivity surfaces where the land surface temperature from MODIS tends to produce a relatively lower temperature than expected creating spuriously high ET values. The approach also needs to be evaluated using data from other sensors such as Landsat and ASTER.

ACKNOWLEDGMENTS

This work was performed under U.S. Geological Survey (USGS) contract G08PC91508 and G10PC00044 in support of the WaterSMART project. The authors are thankful to the journal editor and three anonymous reviewers for their constructive and helpful suggestions to improve the manuscript. They gratefully acknowledge the use of AmeriFlux data for their model validation. The use of trade, firm, or corporation names in this article is for the information and convenience of the reader. Such use does not constitute an official endorsement or approval by the United States Geological Survey or the United States Department of Agriculture or the Agricultural Research Service of any product or service to the exclusion of others that may be suitable.

LITERATURE CITED

Allen, R.G., L.S. Pereira, D. Raes, and M. Smith, 1998. Crop EvapoTranspiration: Guidelines for Computing Crop Water Requirements. *In*: United Nations FAO, Irrigation and Drainage Paper 56, FAO, Rome, Italy.

Allen, R.G., M. Tasumi, A.T. Morse, and R. Trezza, 2005. A Landsat-Based Energy Balance and Evapotranspiration Model in Western US Water Rights Regulation and Planning. ASCE Journal of Irrigation and Drainage Engineering 19:251-268.

Allen, R.G., M. Tasumi, A.T. Morse, R. Trezza, W. Kramber, I. Lorite, and C.W. Robison, 2007a. Satellite-Based Energy Balance for Mapping Evapotranspiration with Internalized Calibration (METRIC) – Applications. ASCE Journal of Irrigation and Drainage Engineering 133(4):395-406.

Allen, R.G., M. Tasumi, and R. Trezza, 2007b. Satellite-Based Energy Balance for Mapping Evapotranspiration with Internalized Calibration (METRIC) – Model. ASCE Journal of Irrigation and Drainage Engineering 133(4):380-394.

Anderson, M.C., J.M. Norman, G.R. Diak, W.P. Kustas, and J.R. Mecikalski, 1997. A Two-Source Time-Integrated Model for Estimating Surface Fluxes Using Thermal Infrared Remote Sensing. Remote Sensing Environment 60:195-216.

Baldocchi, D., E. Falge, L. Gu, R. Olson, D. Hollinger, S. Running, P. Anthoni, C. Bernhofer, K. Davis, R. Evans, J. Fuentes, A. Goldstein, G. Katul, B. Law, X. Lee, Y. Malhi, T. Meyers, W. Munger, W. Oechel, K.T. Paw, K. Pilegaard, H.P. Schmid, R. Valentini, S. Verma, T. Vesala, K. Wilson, and S. Wofsy, FLUXNET, 2001. A New Tool to Study the Temporal and Spatial Variability of Ecosystem-Scale Carbon Dioxide, Water Vapor, and Energy Flux Densities. Bulletin of the American Meteorological Society 82:2415-2434.

Bastiaanssen, W.G.M., M. Menenti, R.A. Feddes, and A.A.M. Holtslag, 1998. The Surface Energy Balance Algorithm for Land (SEBAL): Part 1 Formulation. Journal of Hydrology 212-213:198-212.

Calder, I.R., 1977. A Model of Transpiration and Interception Loss From a Spruce Forest in Plynlimon, Central Wales. Journal of Hydrology 33:247-265.

Gowda, P.H., J.L. Chavez, P.D. Colaizzi, S.R. Evett, T.A. Howell, and J.A. Tolk, 2008. ET Mapping for Agricultural Water Management: Present Status and Challenges. Irrigation Science 26:223-237.

Gowda, P.H., G.B. Senay, P.D. Colaizzi, and T.A. Howell, 2009. Lysimeter Validation of the Simplified Surface Energy Balance (SSEB) Approach for Estimating Actual ET. Applied Engineering in Agriculture. Transactions of ASABE. 25(5):665-669.

Jackson, R.D., D.B. Idso, R.J. Reginato, and P.J. Pinter, 1981. Canopy Temperature as a Crop Water Stress Indicator. Water Resources Research 17:1133-1138.

Kalma, J.D., T.R. McVicar, and M.F. McCabe, 2008. Estimating Land Surface Evaporation: A Review of Methods Using Remotely Sensed Surface Temperature Data. Surveys in Geophysics 29:421-469.

Kanamitsu, M., 1989. Description of the NMC Global Data Assimilation and Forecast System. Weather and Forecasting 4:334-342.

Kustas, W.P. and J.M. Norman, 2000. A Two-Source Energy Balance Approach Using Directional Radiometric Temperature Observations for Sparse Canopy Covered Surfaces. Agronomy Journal 92:847-854.

Moran, M.S., A.F. Rahman, J.C. Washburne, D.C. Goodrich, M.A. Weltz, and W.P. Kustas, 1996. Combining the Penman–Monteith Equation with Measurements of Surface Temperature and Reflectance to Estimate Evaporation Rates of Semiarid Grassland. Agriculture and Forest Meteorology 80:87-109.

Qiu, G.Y., T. Yanob, and K. Momiic, 1998. An Improved Methodology to Measure Evaporation from Bare Soil Based on Comparison of Surface Temperature with a Dry Soil Surface. Journal of Hydrology 210:93-105.

Roerink, G.J., Z. Su, and M. Menenti, 2000. S-SEBI: A Simple Remote Sensing Algorithm to Estimate the Surface Energy Balance. Physics and Chemistry of the Earth 25:147-157.

Senay, G.B., M.E. Budde, and J.P. Verdin, 2011a. Enhancing the Simplified Surface Energy Balance (SSEB) Approach for Estimating Landscape ET: Validation with the METRIC model. Agricultural Water Management 98:606-618.

Senay, G.B., M.E. Budde, J.P. Verdin, and A.M. Melesse, 2007. A Coupled Remote Sensing and Simplified Surface Energy Balance (SSEB) Approach to Estimate Actual Evapotranspiration from Irrigated Fields. Sensors 7:979-1000.

Senay, G.B., S. Leake, P.L. Nagler, G. Artan, J. Dickinson, J.T. Cordova, and E.P. Glenn, 2011b. Estimating Basin Scale Evapotranspiration (ET) by Water Balance and Remote Sensing Methods. Hydrological Processes 25:4037-4049.

Senay, G.B., J.P. Verdin, R. Lietzow, and A.M. Melesse, 2008. Global Reference Evapotranspiration Modeling and Evaluation. Journal of American Water Resources Association 44(4):969-979.

Su, Z., 2002. The Surface Energy Balance System (SEBS) for Estimation of Turbulent Heat Fluxes. Hydrology and Earth System Sciences 6:85-99.

Su, Z., M.F. McCabe, and E.F. Wood, 2005. Modeling Evapotranspiration During SMACEX: Comparing Two Approaches for Local- and Regional-Scale Prediction. Journal of Hydrometeorology 6:910-922.

Wan, Z., 2008. New Refinements and Validation of the MODIS Land-Surface Temperature/Emissivity Products. Remote Sensing Environment 112:59-74.